Heat and Mass Transfer in Hypersaline Geothermal Systems

Curtis Oldenburg, Karsten Pruess, and Marcelo Lippmann

Earth Sciences Division, Lawrence Berkeley Laboratory, Berkeley **CA** 94720, **USA**

keywords: heat transfer, density, double-diffusive convection, porosity, hypersaline

ABSTRACT

Fluid density in hypersaline geothermal systems is controlled by temperature and salinity. For example, brines in the Salton Sea Geothermal System (SSGS) are stably stratified with maximum densities near 1000 kg m $^{-3}$ in the hot. hypersaline regions at depth. In geothermal systems, the porous medium affects double-diffusive convection (free convection with two sources of buoyancy). For example, the permeability of the medium exerts the fundamental control on the flow field. A more subtle effect of the porous medium is to increase the effective diffusivity of the brine through hydrodynamic dispersion. In addition, heat transport is affected by porosity due to heat exchange between the fluid and the solid rock matrix. In forced convection, the increased pore velocity in low-porosity regions enhances brine transport relative to heat transport. In double-diffusive convection, the heat and brine transport are strongly coupled and enhanced transport of brine over heat is limited by density effects. These effects have been investigated using the reservoir simulator TOUGH2 with a newly developed dispersion module (T2DM).

I. INTRODUCTION

Fluid density in hypersaline geothermal systems such as the Salton Sea Geothermal System (SSGS) is controlled by temperature and salinity (Younker et al., 1982; Newmark et al., 1986; and Fournier. 1990). Free convection with two buoyancy sources with different diffusivities is called double-diffusive convection. Double-diffusive convection in systems such as the oceans is generally controlled by the properties of the fluids and the boundary and initial conditions of the system. In geothermal systems, additional effects arise from the porous medium through which the fluid flows. Knowledge of the density and convective behavior of liquid-dominated geothermal systems is critical to efficient energy production.

The porous rock matrix affects double-diffusive convection in at least three ways: (1) hydrodynamic dispersion tends to increase the effective diffusivity of the brine and makes it velocity-dependent; (2) the flow field is strongly controlled by the permeability of the medium; and (3) advective heat transport is retarded due to heat exchange with the solid rock matrix. Prior studies by Rosenberg and Spera (1990) and Rosenberg (1991) discussed the impact of these effects in the context of hydrothermal systems in general.

The purpose of this paper is to further investigate the effects of porosity variation by means of two-dimensional numerical experiments on systems broadly resembling the **SSGS.** We present our model for the density of **SSGS** geothermal brines that is used in the free convection simulations. We briefly discuss the effects of hydrodynamic dispersion in decreasing the contrast in effective diffusivity between the heat and brine components, and the role of permeability in controlling fluid flow. We examine in detail the importance of porosity in the forced convection of heat and brine, and its role in free convection. Although we use an accurate model for the SSGS brine density, the model systems presented here were chosen solely to explore aspects of heat and mass transfer and are not meant to be detailed conceptual models of the **SSGS.**

IT. DENSITY OF GEOTHERMAL ERINES

Because density differences drive double-diffusive convection, it is necessary to have an accurate density model for the numerical experiments. Typical hypersaline SSGS brines contain about 24.6 wt% of NaCl, $CaCl_2$, and KCI with Na-Ca-K molar cation ratios of about .68/.20/.12 (Williams and McKibben, 1989). Although NaCl predominates in the mixture, the presence of $CaCl_2$ is important due to the +2 charge and larger molecular weight of the Ca ion. The +1 charges on Na and K make the effects of these two cations on brine density very similar, and we make the approximation that K can he combined with Na. Thus, we approximate the hypersaline brine as being a 24.6 wt% NaCl-$CaCl_2$ brine with Na-Ca molar ratio of .80/.20. We have used this composition along with unpublished experimental data (C.S. Oakes and J.M. Simonson, pers. comm., 1994) on fluid density in the system NaCl-$CaCl_2$-H_2O to arrive at the density of a single brine component to be used in the numerical model. The data of Oakes and Simonson were collected by vibrating tube densimetry and presented as plots of apparent molar volume (V_ϕ) versus ionic strength. The density of the solution is then calculated by the equation (Oakes et al., 1990)

$$\rho_s = \frac{1000 + \sum_{MX} m_{MX} M_{MX}}{V_\phi \sum_{MX} m_{MX} + \frac{1000}{\rho_w}} \qquad (1)$$

where ρ is in cgs units and the density of water (ρ_w) is calculated after Kestin et al. (1984) and from the steam tables of the International Formulation Committee (1967). (Other symbols are given in the Nomenclature at the end of the paper).

Using the 24.6 wt% brine as the hypothetical brine component end member and the unpublished data of Oakes and Simonson, we find a density of 991 kg m^{-3} at 300 °C and 100 bars. For comparison, a pure NaCl brine of 24.6 wt% NaCl at the same temperature and pressure has a density of 978 kg m^{-3}, while pure $CaCl_2$ brine at the same conditions has a density of 1020 kg m^{-3} (the density of pure water at these conditions is 716 kg m^{-3}). The addition of $CaCl_2$ in the amount present in the SSGS makes brine density differ from pure NaCl brine density (Pitzer et al., 1984) by less than 2% at the same pressure, temperature, and solute concentration.

Following the work of Reeves et al. (1986) and Herbert et al. (1988), we adopt a mixing model in which the aqueous phase consists of two pseudo-components, a hypersaline hrine with mass fraction X_b, and pure water with mass fraction $X_w = 1 - X_b$. The brine "component" is assumed to consist of H_2O, NaCl and $CaCl_2$ in the proportions present in the SSGS. Assuming the volumes of pure water anti brine are additive, we obtain for the mixture density (ρ) the equation

$$\frac{1}{\rho} = \frac{V}{M} = \frac{1 - X_b}{\rho_w} + \frac{X_b}{\rho_b} \qquad (2)$$

where the density of each component is given by $\rho_w = M_w / V_w$ and $\rho_b = M_b / V_b$. The temperature dependence of brine density is calculated using a coefficient of thermal expansivity:

$$\alpha_b = -\frac{1}{\rho_b}\left(\frac{\partial \rho_b}{\partial T}\right) \qquad (3).$$

For pure brine, we define the coefficient of thermal expansivity (α_b) by specifying two reference brine temperatures and densities (ρ_{0b} ; T_{0b}, and ρ_{2b} ; T_{2b}) derived from the unpublished data of Oakes and Simonson. The coefficient of thermal expansivity for the brine is applied through the exponential relation

$$\rho_b = \rho_{0b}\ exp\left[-\alpha_b\,(T-T_{0b})\right] \qquad (4).$$

Subsequent to the calculation of the thermal effects on density for each component, the mixing relation (Eq. 2) is applied to obtain the density of the mixture. The method has been coded as an extension to EOS7, a TOUGH2 thermophysical properties module for pure water, brine and air (Pruess, 1991b).

Plotted in Fig. 1 are results of the above model for the density of SSGS brine as a function of temperature and brine mass fraction (X_b) where X_b = 1.0 corresponds to a 24.6 wt. % NaCl-$CaCl_2$ solution. Pressure is set at 10^5 Pa (1 bar) above the saturation pressure (Psat). Superimposed on the density isopleths are temperature and salinity (TDS) of 45 fluid samples of low TDS, hypersaline, and mixed brines from the SSGS (Williams, 1988; Williams and McKibben, 1989).

The data in Fig. 1 show that temperature and salinity are correlated, and that higher densities occur at hotter (deeper) levels making the reservoir density-stratified. Furthermore, while the SSGS hypersaline brines do indeed have densities of nearly 1000 kg m^{-3}, the densities of less saline brines are generally in the range 850–950 kg m^{-3}.

We note here also that viscosity varies by a factor of two between pure water and pure brine. These effects are incorporated through the correlation (Herbert et al., 1988)

$$f(X_b) = 1 + \mu(1)X_b + \mu(2)X_b^2 + \mu(3)X_b^3 \qquad (5).$$

The viscosity of the brine is calculated by multiplying $f(X_b)$ by the viscosity of pure water at the given pressure and temperature (the values of $\mu(i)$ are given in Table 2).

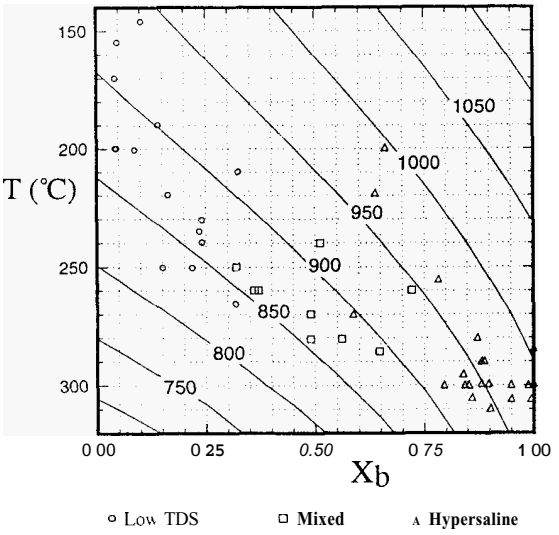

Figure 1. Density (kg m^{-3}) of NaCl-$CaCl_2$ brines as a function of temperature and brine mass fraction. Superimposed are fluid temperature and TDS data for the SSGS from Williams (1988) and Williams and McKibben (1989). The mixed fluids are thought to be mixtures of hypersaline and low-TDS fluids and do not represent true geothermal reservoir conditions.

III. MATHEMATICAL DEVELOPMENT

The general conservation equations governing heat and mass transfer consist of balances of mass accumulation and flux and source terms over **all** grid blocks into which the flow domain has been partitioned:

$$\frac{d}{dt}\int_{V_n} M^{(\kappa)}\,dV = \int_{\Gamma_n} \mathbf{F}^{(\kappa)}\cdot\mathbf{n}\ \ d\Gamma + \int_{V_n} q^{(\kappa)}\,dV$$

Although the TOUGH2 simulator (Pruess, 1987; 1991a) actually includes full multiphase, compressible, and multicomponent flows, we will consider only a single incompressible aqueous phase with water, brine component and heat in the following discussion. The mass accumulation terms for the components κ are written

$$M^{(\kappa)} = \phi\,\rho X^{(\kappa)} \qquad (7)$$

where (κ = 1: water, 2: brine). An analogous accumulation term for the heat component h can be written as

$$M^{(h)} = \phi\,\rho C T + (1-\phi)C_R\rho_R T \qquad (8)$$

where heat exchange occurs between the fluid and the rock matrix (Bodvarsson, 1972). The component fluxes have contributions from Darcy flow, molecular diffusion, and hydrodynamic dispersion and can be written

$$\mathbf{F}^{(\kappa)} = X^{(\kappa)}\,\mathbf{F} - \rho\,\bar{\mathbf{D}}^{(\kappa)}\nabla X^{(\kappa)} \qquad (9).$$

The source term (q) in **Eq.** 6 is zero for the convection scenario of interest. The advective mass flux is given by Darcy's Law

$$\mathbf{F} = \rho\ \mathbf{u} = -\frac{k}{\mu}\rho\left(\nabla P - \rho\,\mathbf{g}\right) \qquad (10)$$

where the density (ρ) is controlled by heat and brine mass fraction. **Eq.** 10 shows that a given buoyancy force produces a given Darcy mass flux. If the porosity is small, the corresponding pore velocity may be large. Permeability variations exert a primary control on the Darcy mass flux and these have been investigated in the context of hydrothermal convection by Rosenberg and Spera (1990).

The dispersion tensor of **Eq.** 9 is written as

$$\bar{\mathbf{D}}^{\kappa} = D_T^{\kappa}\,\bar{\mathbf{I}} + \frac{\left(D_L^{\kappa} - D_T^{\kappa}\right)}{u^2}\,\mathbf{u}\,\mathbf{u}$$

where dispersion is written in terms of dispersion coefficients in the longitudinal (D_L) and transverse (D_T) directions relative to the flow direction, given by

$$D_L^{\kappa} = \phi\cdot\tau\cdot\ d^{\kappa} + \alpha_L\,u \qquad (12)$$

$$D_T^{\kappa} = \phi\cdot\tau\cdot\ d^{\kappa} + \alpha_T\,u \qquad (13).$$

The mass flux of component κ due to molecular diffusion and hydrodynamic dispersion is thus

$$\mathbf{F}_d^{(\kappa)} = -\rho\,D_T^{\kappa}\nabla X^{(\kappa)} - \rho\,\frac{\left(D_L^{\kappa} - D_T^{\kappa}\right)}{u^2}\,\mathbf{u}\,\left(\mathbf{u}\cdot\nabla X^{(\kappa)}\right) \qquad (14).$$

This formulation for hydrodynamic dispersion is coded in T2DM for two-dimensional calculations (Oldenburg and Pruess. 1993).

The total heat flux can be written

$$\mathbf{F}^{(h)} = \rho\,C\,T\ F - K\,V\,T \qquad (15)$$

where we have neglected hydrodynamic dispersion in the heat flux equation. Substituting **Eqs.** 7, 8, 9 and 15 into Eq. 6 and differentiating, we arrive at the two partial differential equations for

advective and dispersive transport of heat and mass components, respectively:

$$\phi \frac{\partial T}{\partial t}\left(1+\frac{(1-\phi)}{\phi}\frac{\rho_R C_R}{\rho C}\right) = -\nabla.\mathbf{u}T + \nabla.\left(\frac{K}{\rho C}\nabla T\right) \qquad (16)$$

$$\phi \frac{\partial X^{(\kappa)}}{\partial t} = -\nabla.\mathbf{u}X^{(\kappa)} + \nabla.\left(\overline{\mathbf{D}}^{(\kappa)}\nabla X^{(\kappa)}\right) \qquad (17)$$

(cf. deMarsily, 1986, p. 277 and 278). We note in Eq. 16 that heat transport is retarded due to the heat exchange between the fluid and the solid grains. The effective thermal retardation factor is given by the ratio of the total heat capacitv of the rock-fluid mixture to the heat capacity of the fluid,

$$R^h = 1 + \frac{(1-\phi)}{\phi}\frac{\rho_R C_R}{\rho C} \qquad (18)$$

Accordingly, as the porosity becomes small, the effective retardation can become vcry large. No retardation is involved for brine transport (Eq. 17); however, mass transport of sorbing species would be subject to similar retardation as heat transport.

For a given Darcy velocity u, pore velocity is u/ϕ, which means that the velocity of the thermal front is

$$v_{th} = \frac{u}{\phi R^h} = u\,\frac{\rho C}{\phi\rho C + (1-\phi)\rho_R C_R} \qquad (19)$$

For porosities typical of geothermal systcms ($\phi \leq .30$) the rock specific heat term dominates, so that for a given Darcy velocity, the propagation of thermal fronts is only weakly dependent on porosity. In contrast, concentration fronts are propagated at the pore velocity, u/ϕ. This leads to the question of what effect variable porosity has on the simultaneous transport of heat and brine. We will investigate this problcm first for forced convection and subsequently for free convection in geothermal system.

We note in passing the importance of hydrodynamic dispersion in increasing the effective diffusivity of the brine component. Specifically, if we substitute into Eqs. 12–14 values for porosity (ϕ) of 0.2, and brine molecular diffusivity (d) of 2×10^{-8} m^2 s^{-1}, and lateral and longitudinal dispersion lengths (α_T and α_L) of 1 and 10 m, wc see from Eqs. 12 and 13 that the hydrodynamic dispersion term becomes of the same order as the molecular diffusion term when the Darcy velocity reaches 4×10^{-9} or 4×10^{-10} m s^{-1}, respectively. Meanwhile, the effective thermal diffusivity is given by the term $K/[\phi\rho C + (1-\phi)\rho_R C_R]$ (see Eq. 16). Substituting the values 1.8 J s^{-1} m^{-1} °C for K, and 1000 kg m^{-3} for ρ, and 4184 J kg^{-1} °C^{-1} for C, 2650 kg m^{-3} for ρ_R, and 1000 J kg^{-1} °C^{-1} for C_R, we find the effective thermal diffusivity is 6.1×10^{-7} m^2 s^{-1}. Thus the effective diffusivity of the brine in the transverse direction will equal the thermal diffusivity when the Darcy velocity equals 6.1×10^{-7} m s^{-1} (about 20 m yr^{-1}). Because many important phenomena in double-diffusive convection occur due to the difference between the diffusivity of the buoyancy-producing components (Veronis, 1965; Huppert and Moore, 1976) and hydrothermal systems can be quite vigorously convecting, the effect of hydrodynamic dispersion on double-diffusive convection in porous media is of critical importance. The full implications of a velocity-dependent effective diffusivity have yet to be investigated.

IV. FORCED CONVECTION

To establish a reference case for our free convection simulations, we present results for a simplified one-dimensional forced convection problem with constant permeability, variable porosity, and fluid viscosity independent of brine mass fraction. The flow system is shown in Fig. 2 and consists of a one-dimensional domain 7 m in length in which brine ($X_b = 1$) is injected non-isothermally under a constant pressure difference which produces a pore velocity of approximately 0.1 m/day. Initially, the system contains pure water ($X_b = 0$) at $T = 25$ °C. Parameters are given in Table 1; temperature and brine mass fraction profiles after $t = 20$ days are presented in Fig. 3. Focusing first on the temperature profiles and comparing the constant porosity results to the variable porosity results, we see in Fig. 3 that the effect of the low-porosity central region is very small. The reason for this is that although heat transport is retarded by the low-porosity region, the pore velocity increases in the central region in order to keep the Darcy mass flux constant. Thus the heat transfer reduced by retardation due to thermal exchange is almost exactly balanced by increased heat transfer due to larger pore velocity in the low-porosity region.

Table 1. Parameters for the forced convection problem (Fig. 2).

property	value	units
pressure [$P(Y = 0\,m)$]	10001.75	Pa
pressure [$P(Y = 7\,m)$]	10000.	Pa
iemperature [$T(Y = 0\,m)$]	45.	°C
temperature [$T(Y = 7m)$]	25.	°C
brine [$X_b(Y = 0\,m)$]	1.	-
brine [$X_b(Y = 7\,m)$]	0.	-
porosity in region 1 (ϕ_1)	.30	-
porosity in region 2 (ϕ_2)	.30 or .03	-
permeability (k)	1.24×10^{-9}	m^2
molecular diffusivity (d)	0.	m^2 s^{-1}
dispersivity (α_L)	1.	m
tortuosity factor (τ)	1.	-
formation conductivity (K)	1.8	J s^{-1} m^{-1} °C^{-1}
heat capacity of rock (C_R)	1030.	J kg^{-1} °C^{-1}
density of rock (ρ_R)	2650.	kg m^{-3}
viscosity coefficient 1 [$\mu(1)$]	0.	–
viscosity coefficient 2 [$\mu(2)$]	0.	–
viscosity coefficient 3 [$\mu(3)$]	0.	–
grid spacing (horizontal)	.20	m

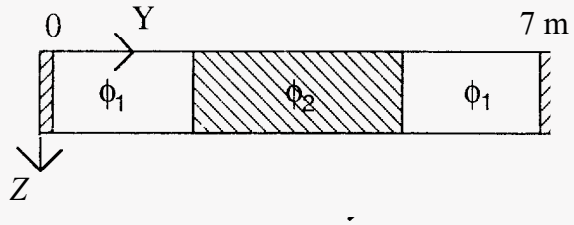

Figure 2. One-dimensional domain for the forced convection test problem. Boundary conditions and parameters are given in Table 1.

From the brine concentration profiles in Fig. 3, we see that the increased pore velocity greatly enhances the brine transport relative to the heat transport. This demonstrates the fundamental difference between heat and mass transport in porous media under conditions of forced convection. When the flow is driven by an externally applied pressure difference, as in this case, the thermal and chemical fronts are free to separate, the separation being controlled by the effects of thermal retardation and increased pore velocity. We will see below that such decoupling cannot occur in free convection where the driving force is buoyancy produced by the components themselves.

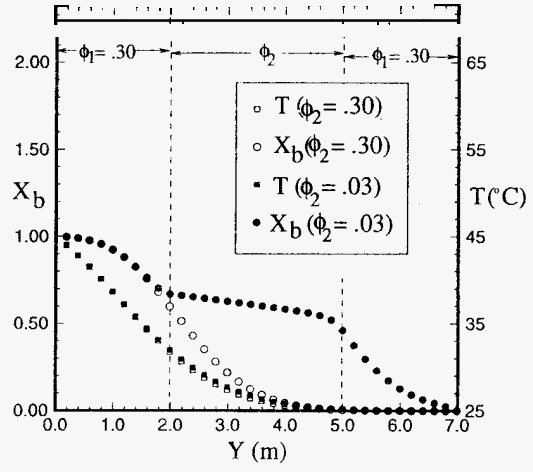

Figure 3. Effects of non-uniform porosity at $t = 20$ days for heat and mass transfer in the one-dimensional forced convection problem.

V. FREE CONVECTION

The effects of porosity on double-diffusive convection in a hypersaline geothermal system like the SSGS are examined in this section. The simulations are carried out with fully implicit time-stepping in TOUGH2. The simulator uses a fully coupled residual-based solution technique that is efficient for strongly coupled flow problems such as double-diffusive convection (Oldenburg and Pruess, 1994). Solution of the resulting system of iinear equations is accomplished with a bi-conjugate gradient solver (Moridis et al., 1994).

The domain, boundary and initial conditions for the system we consider are shown in Fig. **4** and the parameters are presented in Table 2. Prior simulation results for the SSGS (Oldenburg et al., 1994) did not include the dependence of viscosity on brine mass fraction. We observe in the present simulations longer convective time scales due to the larger fluid viscosity of the concentrated brine (Eq. 5). Note also that we use an anisotropic permeability with $k_Y = 100\,k_Z$. We emphasize that although we have used an accurate model for the density of the fluids and the parameters are chosen to be representative of the SSGS, the system modeled should not be considered a conceptual model for the SSGS, but rather a hypothetical system for illustrating the effects of porosity on double-diffusive convection.

Fig. *5* shows vectors of pore velocity with temperature, brine mass fraction, and density fields for a constant permeability and constant porosity system ($\phi = 0.2$) at t = 30,000 yrs. Note in Fig. *5* that the thermal plume and brine plume rise to approximately the same height. Even though heat transport is subject to retardation, the heat and brine plumes rise together. From a more detailed examination of Fig. *5*, the mechanism forcing thermal and brine plumes to occupy the same region is explained as follows. **As** hotter and more saline fluid is convected upwards, the front of higher concentration brine advances ahead of the (hot) temperature front because of thermal retardation. Therefore, at the leading edge of the plume fluid density increases, diminishing the upward buoyancy force. The more concentrated brine cannot advance beyond the region of increased temperature due to lack of positive buoyancy. A similar phenomenon has been observed in laboratory experiments of upward brine transport, where diminished buoyancy of higher brine concentrationc resulted in smaller dispersivity (sharper fronts) (Fein, 1991). Thus we observe that heat and brine transport are closely tied together even though heat transport is retarded and brine transport is not.

In Fig. 6 we show results for a case with increased thermal retardation ($\phi = 0.02$) at t = 30,000 yrs. Comparison of the isopleths of Figs. *5* and *6* reveals their similarity and leads to the tentative conclusion that for conditions of constant permeability, double-diffusive convection is largely independent of porosity (the vectors are pore velocity and are correspondingly larger in Fig. **6).** It is interesting to consider why a convective system driven by the buoyancy due to temperature and concentration effects should be independent of porosity when the transport of heat alone is greatly retarded by the rock matrix, while brine migration is accelerated for low porosities. The keys to this question are (1) the approximate balance between pore velocity and thermal retardation associated with the porosity of the rock matrix as seen in forced convection (Eq. 19, Fig. 3), and (2) the density "lid" that is produced by the advancing brine front. Specifically, a given buoyancy force produces a given Darcy mass flux which results in a pore velocity that is inversely proportional to porosity. At the same time, the retardation of heat transport is directly proportional to the fraction of the medium occupied by rock ($1 - \phi$). The effects of increased pore velocity and increased thermal retardation in a lower-porosity region approximately cancel one another (Eq. 19). As seen in forced convection, the higher pore velocity in the low-porosity system results in the tendency for accelerated brine transport. However, in free convection, it appears that the accelerated brine transport produces a density lid on the system as discussed above, preventing the thermal and brine plumes from separating.

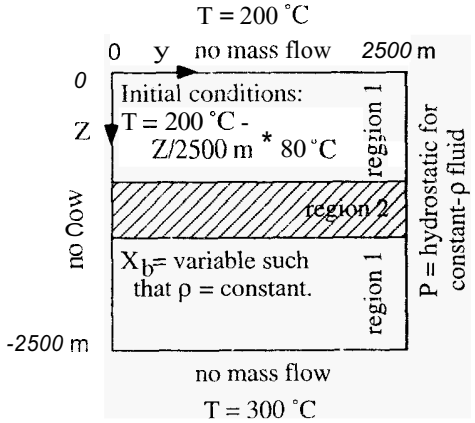

Figure **4.** Domain and boundary and initial conditions for the free convection problem. The initial temperature profile is linear, while the initial brine mass fraction profile is adjusted such that the density of the liquid is exactly 925 kg m^{-3}.

Table 2. Parameters *for* the free-convection problem (Fig. *4).*

quantity	value	units
porosity (ϕ_1)	.2	–
porosity (ϕ_2)	.2 or .02	–
permeability (k_Y)	5 x 10^{-13}	m^2
permeability (k_Z)	5 x 10^{-15}	m^2
molecular diffusivity (d)	2x 10^{-8}	m^2 s^{-1}
transversal dispersivity (α_T)	1.	m
longitudinal dispersivity (α_L)	10.	m
tortuosity factor (τ)	1.	–
formation heat conductivity (K)	1.8	J s^{-1} m^{-1} °C^{-1}
heat capacity of rock (C_R)	1000	J kg^{-1} °C^{-1}
density of rock (ρ_R)	2650.	kg m^{-3}
density of brine (at 200 °C) (ρ_{0b})	1077.	kg m^{-3}
density of brine (at 300 °C) (ρ_{2b})	991.	kg m^{-3}
viscosity coefficient 1 ($\mu(1)$)	.4819	–
viscosity coefficient 2 ($\mu(2)$)	-.2774	
viscosity coefficient 3 ($\mu(3)$)	.78 14	–
grid spacing (horizontal)	100	m
grid spacing (vertical)	100	m

To further demonstrate these effects, we present in Fig. 7 results for a constant permeability domain with a low-porosity layer (ϕ_2 = 0.02) in region 2 (Fig. **4**; -1500 m < Z < -1000 m) at t = 30,000 yrs. Note first in Fig. 7 that because a given buoyancy force produces a given Darcy mass flux (see **Eq.** 10), vectors of pore velocity are larger in the low-porosity region. Nevertheless, comparison of the temperature, brine concentration, and density fields of Figs. *5,* **6** and 7 shows that the low-porosity layer has a limited effect and double-diffusive convection is only slightly affected by porosity. Thus it appears that convective heat and mass transfer is largely independent of porosity.

VI. CONCLUSIONS

An accurate model for brine density as a function of temperature and NaCl-CaCl$_2$ concentration reveals that the SSGS is density stratified with average density of about 925 kg m^{-3}. Analysis of the brine transport equations reveals that hydrodynamic dispersion enhances the effective diffusivity of brine making the contrast between the effective diffusivities of heat and brine negligible at commonly occurring convective velocities. Because many important phenomena in double-diffusive convection such as layered, chaotic and oscillatory convection are produced by the difference in diffusivities between the buoyancy-producing components, the effect of hydrodynamic dispersion is fundamental to porous media double-diffusive convection.

Numerical simulation reveals that for forced convection, low porosity enhances brine transport relative to heat transport and the two fronts separate; heat transfer alone is little affected by porosity due to the competing effects of thermal retardation and higher pore velocity.

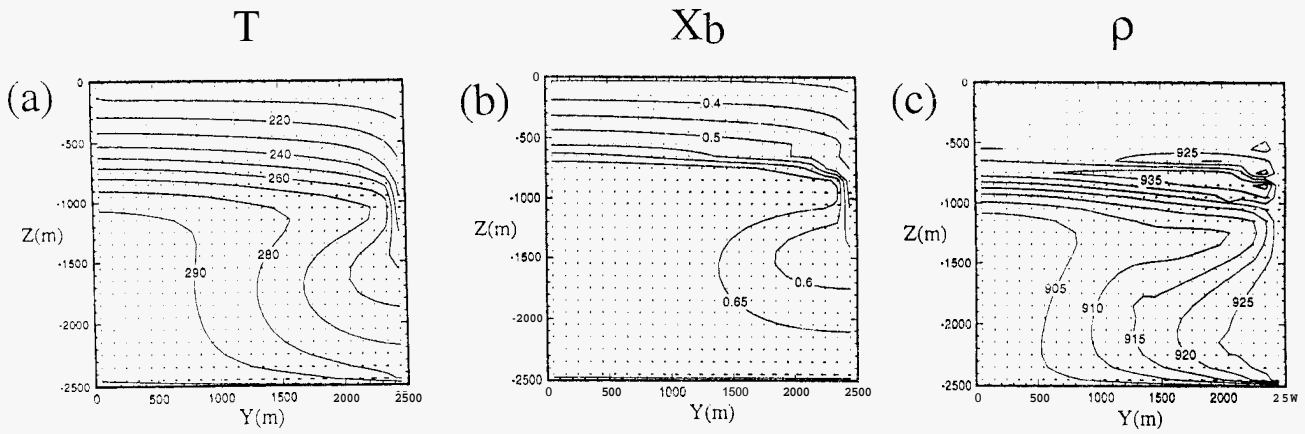

Figure 5. Free convection results with constant porosity ($\phi = 0.20$) at $t = 30{,}000$ yrs. (a) temperature (°C); (b) brine mass fraction (X_b); and (c) density (kg m^{-3}). Vectors show pore velocity.

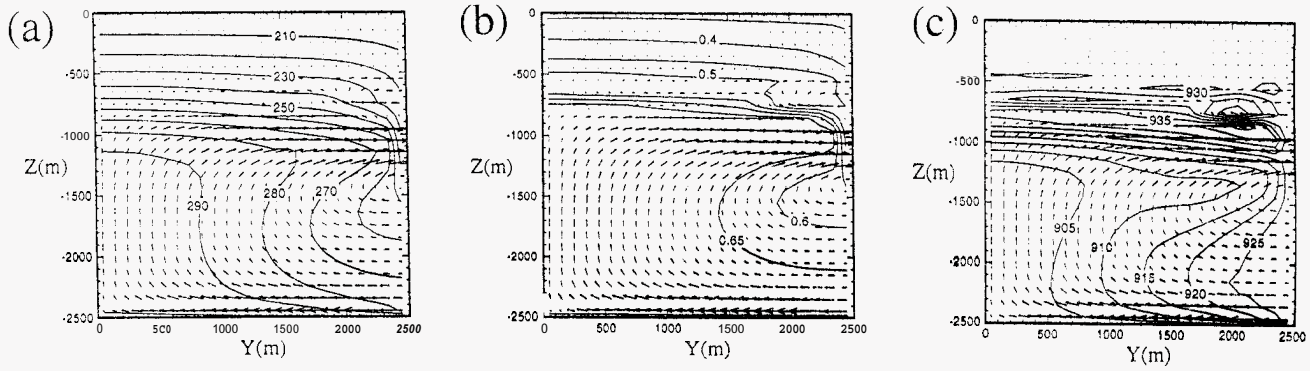

Figure 6. Free convection results with constant porosity ($\phi = 0.02$) at $t = 30{,}000$ yrs. (a) temperature ("C); (b) brine mass fraction (X_b); and (c) density (kg m^{-3}). Vectors show pore velocity

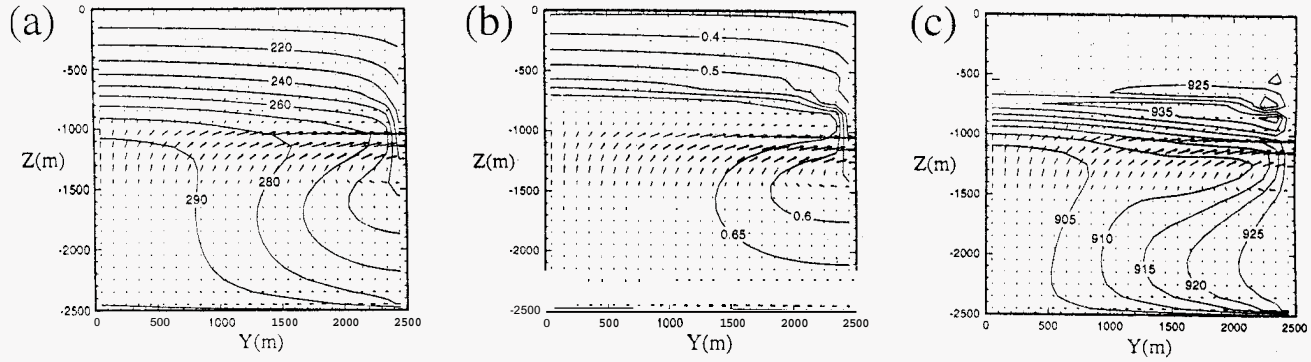

Figure 7. Free convection results with low-porosity layer (Region 2; Fig. 4; $\phi_2 = 0.02$) at $t = 30{,}000$ yrs. (a) tempcrature ("C); (b) brine mass fraction (X_b); and (cj density (kg m^{-3}) Vectors show pore velocity.

In free convection, where buoyancy produced by temperature and brine concentration differences drive the flow, there is little enhanced transport of brine relative to heat due to thermal retardation. This occurs for two reasons: (1) in a low-porosity region, heat transport is not greatly affected due to the competing effects of thermal retardation and increased pore velocity; and *(2)* the increased density at the top of the plume associated with the faster advance of the brine front causes fluid to resist moving upward and produces an effective lid on the thermal and brine plumes. This behavior underscores the difference between the decoupled equations of forced convection and the strongly coupled nature of double-diffusive convection. It should be pointed out that in natural systems the permeability may be smaller in the low-porosity regions, which would produce smaller convective velocities and thus decrease heat and mass transport across the layer.

Acknowledgments

Special thanks go to Charles S. Oakes for providing a set of unpublished density data and assisting with its interpretation. We thank Stefan Finsterle and Teklu Hadgu for thoughtful reviews. This work was supported by the Assistant Secretary for Energy Efficiency and Renewable Energy, Geothermal Division, **of** the **U.S.** Department of Energy under Contract No. DE-AC03-76SF00098.

Nomenclature

C	heat capacity	J kg^{-1} °C^{-1}
d	molecular diffusivity	m^2 s^{-1}
D	dispersion coefficient	m^2 s^{-1}
D	dispersion tensor	m^2 s^{-1}

$\mathbf{g}$	acceleiation of gravity vector	$m\ s^{-2}$
$\mathbf{F}$	Darcy flux vector	$kg\ m^{2}\ s^{-1}$
h	heat component	J
$\mathbf{I}$	identity matrix	-
k	permeability	m^{2}
K	thermal conductivity	$J\ s^{-1}\ m^{-1}\ °C^{-1}$
m	molality	$mol\ gm^{-1}$
M	mass	kg
MW	molecular weight	$gm\ mol^{-1}$
M_b	mass of brine	kg
$\mathbf{n}$	outward unit normal vector	-
P	total pressure	Pa
q^h	source term	$kg\ s^{-1}$
R	effective retardation factor	-
t	time	years
T	temperature	°C
u	magnitude of Darcy velocity vector	$m\ s^{-1}$
$\mathbf{u}$	Darcy velocity vector	$m\ s^{-1}$
v_{th}	velocity of thermal front	$m\ s^{-1}$
V	volume	m^{3}
V_ϕ	apparent molar volume	$m^{3}\ mol^{-1}$
X	mass fraction	-
Y	Y-coordinate	m
Z	Z-coordinate (positive upward)	m

Greek symbols

α	intrinsic dispersivity	m
α_b	thermal expansivity of brine	$°C^{-1}$
μ	dynamic viscosity	$kg\ m^{-1}\ s^{-1}$
ϕ	porosity	
Γ	grid block interface area	m^{2}
ρ	density	$kg\ m^{-3}$
τ	tortuosity	

Subscripts and superscripts

b	brine
d	dispersion
h	heat
L	longitudinal
MX	salt (M: cations; X: anions)
n	grid block index
R	rock
s	solution
T	transversal
w	water
κ	mass components
$0b$	first reference value for brine
$2b$	second reference value for brine

REFERENCES

Bodvarsson, G., Thermal problems in the siting of reinjection wells, *Geothemics, I* (2), 63–66, 1972.

deMarsily, G., *Quantitative Hydrogeology*, Academic Press, San Diego, CA, **pp.** 230-247, 1986.

Fein, E., Brine transport in porous media at high salinity, GSF Institut für Tieflagerung Abteilung fur Endlagersicherheit, GSF-Bericht 5/91, 1991.

Fournier, R.O., Double-diffusive convection in geothermal systems: The Salton Sea, California, geothermal system as a likely candidate, *Geothemics, 19*(6), 481–496, 1990.

Herbert, A.W., Jackson, C.P. and Lever, D.A., Coupled groundwater flow and solute transport with fluid density strongly dependent on concentration, *Water Res. Res., 24* (IO), 1781-1795, 1988.

Huppert, H.E. and Moore, D.R., Nonlinear double-diffusive convection, *J. Fluid Mech., 78,* 821–854, 1976.

International Formulation Committee, **A** formulation of the thermodynamic properties of ordinary water substance, IFC Secretariat, Diisseldorf, Germany, 1967.

Kestin, J., Sengers, J.V., Kamgar-Parsi, B. and Levelt Sengers, J.M.H., Thermophysical properties of fluid H_2O, *The Journal of Physical and Chemical Reference Data, 13*(1), 175-183, 1984.

Moridis, G.J., Antunez, E. and Pruess, K., "**A** package of preconditioned conjugate gradient solvers for TOUGH2, *Lawrence Berkeley Laborutory Report LBL- 35518,* 1994.

Newmark, R.L., Kasameyer, P.W., Younker, L.W. and Lysne, P.C., Research drilling at the Salton Sea Geothermal Field, California: The shallow thermal gradient project, *Transactions of the American Geophysical Union EOS*, *67*(39), 698–707, 1986.

Oakes, C.S., Simonson, J.M. and Bodnar, R.J., The system NaCl-$CaCl_2$-H_2O. 2. Densities for ionic strengths of 0.1–19.2 mol kg^{-1} at 298.15 and 308.15 K and at 0.1 MPa, *J. of Chemical & Engineering Datu, 35*, 304–309, 1990.

Oldenburg, C.M. and Pruess, K., **A** two-dimensional dispersion module for the TOUGH2 simulator, *Luwrence Berkeley Laboratory Report LBL-* 32505, 1993.

Oldenburg, C.M. and Pruess, K., Dispersive transport dynamics in a strongly coupled groundwater-brine flow system, *Wat. Res. Res,,* in press, 1994.

Oldenburg, C.M., Pruess, K. and Lippmann, M., Double-diffusive convection in liquid-dominated geothermal systems with high-salinity brines, Paper presented at 19th Workshop on Geothermal Reservoir Engineering, Stanford University, January 18–22, 1994, and *Luwrence Berkeley Laboratory Report LBL-* 35039, 1993.

Pitzer, **K.S.,** Peiper, J.C. and Busey, R.H., Thermodynamic properties of aqueous sodium chloride solutions, *J. Phys. and Chem. Ref. Data, 13*(1), 1–102, 1984.

Pruess, K., TOUGH User's Guide, Nuclear Regulatory Commission, Report NUREG/CR-4645, June 1987 (also *Luwrence Berkeley Laboratory Report, LBL-20700,* June 1987).

Pruess, K., TOUGH2 - A General Purpose Numerical Simulator for Multiphase Fluid and Heat Flow, *Lawrence Berkeley Laboratory Report LBL-29400,* May 1991a.

Pruess, K., EOS7, An equation-of-state module for the TOUGH2 simulator for two-phase flow of saline water and air, *Lawrence Berkeley Laboratory Report LBL-31114,* August 1991b.

Reeves, M., Ward, D.S., Johns, N.D. and Cranwell, R.M., Theory and implementation of SWIFT II, the Sandia Waste-Isolation Flow and Transport Model for Fractured Media, *Report* No. *SAND83-1159*, Sandia National Laboratories, Albuquerque, N.M., 1986.

Rosenberg, N.D., Numerical studies of fluid flow and heat and solute transport in hydrothermal systems, Ph.D. dissertation, University of California, Santa Barbara, 138p., 1991.

Rosenherg, N.D. and Spera, F.J., Role of anisotropic and/or layered permeability in hydrothermal convection, *Geophys. Res. Letters, 17*(3), 235–238, 1990.

Veronis, G., On finite amplitude instability in thermohaline convection, *J. Mar. Res., 23,* 1–17, 1965.

Williams, A.E., Delineation of a brine interface in the Salton Sea Geothermal System, California, *Geothermal Resources Council, Transactions, 12,* 151–157, 1988.

Williams, A.E. and McKibben, M.A., A brine interface in the Salton Sea geothermal system, California: Fluid geochemical and isotopic characteristics, *Geochimica et Cosmochimica Acta*, *53,* 1905–1920, 1989.

Younker, L.W., Kasameyer, P.W. and Tewhey, J.D., Geological, geophysical, and thermal characteristics of the Salton Sea Geothermal Field, California, *J. Volcanol. Geotherm. Res., 12,* 221–258, 1982.